Alzheimer's disease BIN1 coding variants increase intracellular Aβ levels by interfering with BACE1 recycling

Catarina Perdigão, Mariana A. Barata, Tatiana Burrinha[ID], and Cláudia Guimas Almeida*[ID]
From the iNOVA4Health, CEDOC, NOVA Medical School, NMS, Universidade Nova de Lisboa, Lisboa, Portugal

Edited by Paul Fraser

Genetic studies have identified BIN1 as the second most important risk locus associated with late-onset Alzheimer's disease (LOAD). However, it is unclear how mutation of this locus mechanistically promotes Alzheimer's disease (AD) pathology. Here we show the consequences of two coding variants in BIN1 (rs754834233 and rs138047593), both in terms of intracellular beta-amyloid (iAbeta) accumulation and early endosome enlargement, two interrelated early cytopathological AD phenotypes, supporting their association with LOAD risk. We previously found that Bin1 deficiency potentiates iAbeta production by enabling BACE1 cleavage of the amyloid precursor protein in enlarged early endosomes due to decreased BACE1 recycling. Here, we discovered that the expression of the two LOAD mutant forms of Bin1 does not rescue the iAbeta accumulation and early endosome enlargement induced by Bin1 knockdown and recovered by wild-type Bin1. Moreover, the overexpression of Bin1 mutants, but not wild-type Bin1, increased the iAbeta42 fragment by reducing the recycling of BACE1, which accumulated in early endosomes, recapitulating the phenotype of Bin1 knockdown. We showed that the mutations in Bin1 reduced its interaction with BACE1. The endocytic recycling of transferrin was similarly affected, indicating that Bin1 is a general regulator of endocytic recycling. These data demonstrate that the LOAD-coding variants in Bin1 lead to a loss of function in endocytic recycling, which may be an early causal mechanism of LOAD.

Alzheimer's disease (AD) is the most common neurodegenerative disease worldwide. The earliest known mechanisms driving AD predicted to begin decades before diagnoses are beta-amyloid (Aβ) intracellular accumulation and endosome dysfunction (1, 2). Aβ is generated intracellularly through the sequential processing of the transmembrane amyloid precursor protein (APP) by β-secretase 1 (BACE1) and γ-secretase (3–6). APP cleavage by BACE1 is the rate-limiting step to generate Aβ (4). Interestingly, APP and BACE1 segregate in the plasma membrane (7, 8). Endocytosis potentiates the encounter of APP and BACE1, and processing, by delivery to a common early endosome (7, 9–12). Aβ production is counteracted by APP sorting for degradation (13–15) and BACE1

recycling to the plasma membrane (8, 15). Endosomal dysfunction causes are unclear. In familial AD (FAD), autosomal mutations cause increased Aβ42 production (16–19), which we and others implicated in endosomal abnormalities (20–23). In late-onset AD (LOAD), the causal mechanisms of Aβ intracellular accumulation and endosomal enlargement are likely different. LOAD is expected multifactorial, caused by a combination of aging, lifestyle, and genetic risk factors. Geneticists have been looking for genetic risk factors in LOAD patients, given the prediction for a strong genetic predisposition, 58–79% (24). Among the genetic risk factors identified by several genome-wide association studies (GWAS), *BIN1*, bridging integrator 1, was the second most associated with increased AD risk (24–30).

BIN1 encodes several isoforms and, in the brain, are mainly expressed the neuronal and ubiquitous isoforms (31). Bin1 belongs to the BAR (Bin1/amphiphysin/RVS167) superfamily. Bin1 isoforms share the N-BAR domain, responsible for sensing and inducing curvature of membranes (32, 33), and the SH3 domain, responsible for interacting with several endocytic players, such as dynamin (34–37), involved in the scission of budding vesicles. The neuronal-specific isoform also encodes the CLAP (clathrin and AP2 binding) domain, responsible for interacting with clathrin and AP2 (38), both required for clathrin-mediated endocytosis. In nonneuronal cells, Bin1 overexpression inhibits transferrin endocytosis, known to be mediated by clathrin (37). Furthermore, Bin1 knockdown reduces transferrin receptor recycling but not its endocytosis (39, 40). In neurons, we previously showed that Bin1 polarizes to axons, associated with early endosomes (15).

In AD, how Bin1 levels change is still controversial. *BIN1* transcripts increase in AD human brains (41). However, lower *BIN1* transcripts correlate with earlier disease onset (42). In FAD models, Bin1 protein accumulates adjacent to amyloid plaques (43). In contrast, in LOAD human brain homogenates, Bin1 protein levels decrease (44, 45) or are unchanged (46). An analysis of Bin1 isoforms separately revealed that neuronal Bin1 decreases while ubiquitous Bin1 increases in AD human brains (47, 48).

To study the impact of Bin1 depletion, researchers have taken a knockdown approach *in vitro* because the Bin1 mouse knockout is perinatal lethal (39). Bin1 knockdown in cortical neurons increases Aβ42 intracellular production (15, 49). In addition, Bin1 knockdown reduces endocytic BACE1 recycling

* For correspondence: Cláudia Guimas Almeida, claudia.almeida@nms.unl.pt.

(15), probably enlarging early endosomes (15, 50). Mechanistically, Bin1 contributes to the scission of recycling carriers containing BACE1 from early endosomes (15). *In vivo* Aβ accumulation was undetectable in mice conditionally knocked out for Bin1 in excitatory neurons (51), indicating that Bin1 does not control the Aβ production in excitatory neurons or the intracellular Aβ accumulation is difficult to detect *in vivo* (52). These findings support Bin1 loss of function in AD, implicated in AD earliest mechanisms in neurons: Aβ intracellular accumulation and endosomal abnormalities.

The impact of Bin1 accumulation in AD is less studied. Increased Bin1 expression decreases early endosomes size (50), opposite to AD early endosome enlargement but possibly linked to tau spreading, a mechanism related to AD progression. However, whether Bin1 increased levels impact Aβ42 intracellular accumulation is still not known.

GWAS and subsequent targeted sequencing associated *BIN1* variants, in regulatory and coding regions, with LOAD and poorer memory performance (24–29, 31, 53, 54). While the regulatory variants may be more frequent and likely associated with alterations in Bin1 transcription, the impact of the coding variants in Bin1 is unknown. Two coding variants leading to mutations in Bin1 were associated with LOAD (53, 55). The first identified was rs754834233 (P318 L (PL)), a proline for a leucine mutation localized to the proline-serine-rich domain proximal to the CLAP domain (55). The second mutation identified was rs138047593 (K358 R (KR)), an arginine for a lysine mutation within the Bin1 SH3 domain (53). Both mutations locate in or near domains necessary for Bin1 proper function at endocytosis and recycling.

We set out to investigate if two LOAD Bin1 mutations interfere with Bin1 function and lead to LOAD earliest mechanisms, Aβ intracellular accumulation, and endosomal abnormalities. We mutagenized wild-type Bin1 with LOAD Bin1 PL and KR mutations. We used an overexpression and rescue approach in the neuronal N2a cell line. By analyzing endogenous intracellular Aβ42 accumulation, BACE1 endocytic trafficking, and early endosome size, we found that PL and KR replicate the impact of Bin1 loss of function. Thus, these mutations may contribute to the development of LOAD early mechanisms.

Results

Bin1 mutants increase intracellular Aβ42 accumulation

Previously, we found that Bin1 loss of function results in Aβ42 intracellular accumulation in a neuroblastoma cell line (N2a) and murine primary neurons (15). Significantly, this defect was only rescued by Bin1 neuronal isoform (15), revealing a specific function of neuronal Bin1 in Aβ42 production. We now want to understand if rare coding variants that lead to mutations in Bin1 found associated with LOAD are sufficient to increase Aβ42 intracellular accumulation. Besides, we investigated if neuronal Bin1 increased levels also interfere with Aβ42 accumulation. To do so, we used a semiquantitative assay for intracellular endogenous Aβ based on Aβ42 immunofluorescence that we performed previously

(15, 20, 52). We have controlled this assay extensively, including with APP knockout cells (56). Here, we show that Aβ42 immunofluorescence was significantly reduced (50%) upon inhibition of Aβ production (Fig. S1, *A* and *B*). We introduced PL and KR mutations, in the corresponding nucleotides, in mouse neuronal MYC-tagged BIN1 cDNA (Bin1-PL and Bin1-KR, respectively). We overexpressed (OE) either neuronal Bin1 wild-type (Bin1-WT), Bin1-PL, Bin1-KR, or MYC-empty vector (MYC) in N2a cells. We observed that overexpressed Bin1-PL and KR have a broad cellular distribution similar to overexpressed Bin1-WT (Fig. 1A) but different from endogenous Bin1, which localizes to early endosomes (15). We found that Bin1-WT overexpression did not change intracellular endogenous Aβ42 levels (Fig. 1, *A* and *B*). In contrast, Bin1-PL and Bin1-KR overexpression increased intracellular Aβ42 significantly, in 12% and 30%, respectively. Since the fluorescence of Aβ42 increased in areas of high anti-MYC fluorescence, we analyzed at higher resolution the fluorescence profiles of Aβ42, Bin1-WT, Bin1 mutants, or MYC vector and found that the fluorescence peaks do not entirely overlap (Fig. S1, *C* and *D*). Moreover, we verified that the anti-MYC immunofluorescence mean intensity was unchanged when Aβ42 mean intensity was reduced (Fig. S1, *A* and *B*).

To understand whether Bin1 mutants induced Aβ42 accumulation in early or late endosomes/lysosomes, we assessed Aβ42 colocalization with EEA1- or LAMP1-positive endosomes, respectively. We found that Bin1-KR increased Aβ42 in EEA1-and LAMP1-positive endosomes, while the Bin1-PL only increased Aβ42 in LAMP1-positive endosomes (Fig. S2, *A* and *B*). Overall, the data indicate that Bin1 mutants increase Aβ42 more in late endosomes/lysosomes (40%) than in early endosomes (30%). This trend is in agreement with our previous observations in primary neurons modeling familial AD (21).

To confirm if the rise in Aβ accumulation was specific for Aβ42, the most toxic Aβ, we evaluated the effect of Bin1-WT and mutants' overexpression in intracellular Aβ40 (Fig. 1, *C* and *D*). Indeed, we found that Bin1-PL overexpression decreased Aβ40 (15%), and the Bin1-KR overexpression reduced more Aβ40 (25%), in contrast to the observed increase in Aβ42. Of note, Bin1-WT overexpression showed no significant impact on Aβ40 levels. Together these results suggest that Bin1 mutants may contribute to an increased ratio of Aβ42 over 40, potentially linked to higher Aβ toxicity (57).

The increase in Aβ42 accumulation upon Bin1 mutants' overexpression recapitulates the impact of Bin1 knockdown (KD) (15, 49), suggesting that the PL and KR mutations lead to Bin1 loss of function.

To verify if these mutations lead to a loss of function, we eliminated the confounding role of endogenous Bin1 by expressing siRNA-resistant Bin1-WT or Bin1 mutants in cells treated with Bin1 siRNA (knockdown). The localization of Bin1 mutants was similar to Bin1-WT when expressed in Bin1 knockdown (KD) cells (Fig. 1E). Importantly, we observed that the mutants did not rescue the rise in Aβ42 levels induced by Bin1 KD, as the neuronal Bin1-WT (15) (Fig. 1, *E* and *F*). This
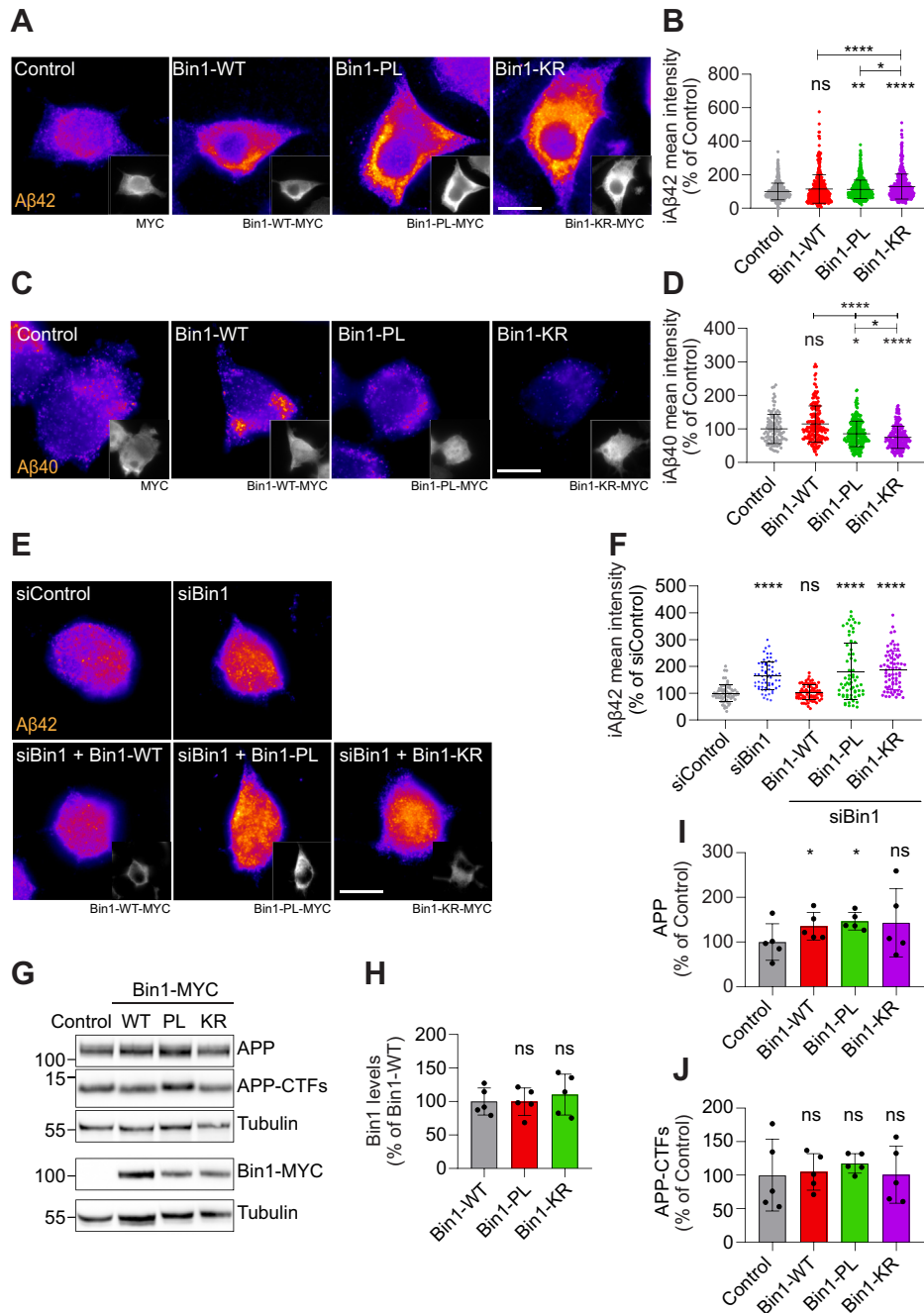
Figure 1. BIN1 mutants increase intracellular Aβ accumulation. *A*, intracellular endogenous Aβ42 (fire LUT) in N2a cells transiently expressing Bin1 wild-type (WT), Bin1 mutants PL and KR tagged with MYC, or MYC (control), immunolabeled with anti-Aβ42 and anti-MYC (*insets*), analyzed by epifluorescence microscopy. Scale bar, 10 μm. *B*, quantification of mean Aβ42 fluorescence intensity relative to control cells (n = 4, $N_{control}$ = 492 cells, $N_{Bin1-WT}$ = 410 cells, $N_{Bin1-PL}$ = 564 cells, $N_{Bin1-KR}$ = 530 cells; *p = 0.0284 Bin1-PL *versus* Bin1-KR, **p = 0.0018 Bin1-PL *versus* control, ****p < 0.0001 Bin1-WT *versus* Bin1-KR, Bin1-KR *versus* control, Kruskal–Wallis test, mean ± SD). *C*, intracellular endogenous Aβ40 (fire LUT) in N2a cells transiently expressing Bin1 wild-type (WT), Bin1 mutants PL and KR tagged with MYC, or MYC (control), immunolabeled with anti-Aβ40 and anti-MYC (*insets*), analyzed by epifluorescence microscopy. Scale bar, 10 μm. *D*, quantification of mean Aβ40 fluorescence intensity relative to control cells (n = 3, $N_{control}$ = 114 cells, $N_{Bin1-WT}$ = 187 cells, $N_{Bin1-PL}$ = 251 cells, $N_{Bin1-KR}$ = 224 cells; [ns]P = 0.2287 Bin1-WT *versus* control, *p = 0.0333 Bin1-PL *versus* control, ****p < 0.0001 Bin1-WT *versus* control, ****p < 0.0001 Bin1-PL *versus* Bin1 -WT, ****p < 0.0001 Bin1-KR *versus* Bin1-WT, *p = 0.0333 Bin1-KR *versus* Bin1-PL, Kruskal–Wallis test, mean ± SD). *E*, intracellular endogenous Aβ42 (fire) in siControl- and siBin1-treated N2a cells followed by transient transfection of Bin1-WT or Bin1 mutants PL and KR tagged with MYC. N2a cells immunolabeled with anti-Aβ42 (*upper panel*) and anti-MYC (*lower panel*), analyzed by epifluorescence microscopy. Scale bar, 10 μm. *F*, quantification of intracellular Aβ42 (iAβ42) mean fluorescence in percentage of siControl (n = 3, $N_{siControl}$ = 64 cells, N_{siBin1} = 63 cells, $N_{siBin1+Bin1-WT}$ = 65 cells, $N_{siBin1+Bin1-PL}$ = 67 cells, $N_{siBin1+Bin1-KR}$ = 72 cells; ****p < 0.0001 siBin1 *versus* siControl, siBin1+Bin1-PL *versus* siControl, siBin1+Bin1-KR *versus* siControl, Kruskal–Wallis test, mean ± SD). *G*, endogenous APP and APP-CTFs levels by western blot with anti-APP antibody (Y188) of N2a cells transiently expressing Bin1-WT, or Bin1-PL and -KR tagged with MYC, or MYC (control). Bin1 expression was analyzed by western blot with anti-MYC antibody. MYC empty vector was not detectable due to its small size. Tubulin was immunoblotted as the loading control. *H*, quantification of Bin1-WT, Bin1-PL, and Bin1-KR levels normalized to tubulin in the percentage of Bin1-WT (n = 5, [ns]P = 0.8649 Bin1-KR *versus* Bin1-WT, [ns]P = 0.9829 Bin1-PL *versus* Bin1-WT, RM one way-ANOVA, mean ± SD). *I*, quantification of APP levels normalized to tubulin in percentage of control (n = 5, [ns]P = 0.2236 Bin1-KR *versus* control, *p = 0.0227 Bin1-PL *versus* control, *p = 0.0171 Bin1-WT *versus* control, paired *t* test, mean ± SD). *J*, quantification of APP-CTFs levels normalized to tubulin in the percentage of control (n = 5, [ns]P = 0.9831 Bin1-PL *versus* control, [ns]P = 0.9965 Bin1-WT *versus* control, Bin1-KR *versus* control, RM one way-ANOVA, mean ± SD).

result supports that the LOAD mutations cause a loss of function of Bin1 in the control of Aβ production.

To understand if increased APP processing underscored the rise in Aβ42, we investigated APP processing into its C-terminal fragments (APP-CTFs). APP processing was analyzed by western blot using the antibody Y188 against the C-terminal domain of APP, detecting APP full-length and the APP-CTFs. We did not see changes in the level of endogenous APP-CTFs when expressing Bin1-WT or its mutants (Fig. 1, *G* and *J*). Instead, we found APP full-length increased upon Bin1-WT (35%) and Bin1-PL (46%) but not Bin-KR overexpression (Fig. 1*I*). This increase in APP full-length does not correlate with the observed rise in Aβ levels. While Aβ is higher with the KR mutant, APP full-length is not. We also observed that Bin1 mutants did not change Bin1 expression levels (Fig. 1, *G* and *H*). Since Bin1-WT OE decreases early endosomes (50), it could decrease sorting at early endosomes for lysosomal degradation, explaining the increase in APP levels.

Bin1 mutants lose control of early endosomes size

Next, we investigated if the LOAD mutations in Bin1 lead to endosomal abnormalities, namely endosomal enlargement, another early LOAD mechanism. Previous work demonstrated that Bin1 controls early endosome size since Bin1 KD increases it and neuronal Bin1 OE reduces it (15, 50).

To investigate how Bin1 mutants affect early endosome size, we transiently expressed Rab5-GFP, an RAB GTPase enriched at early endosomes, overexpressed Bin1-WT, Bin1-PL, Bin1-KR, and MYC as control, and measured Rab5-positive endosome size in N2a cells. As previously reported, Bin1-WT OE decreased Rab5-positive endosome size by 20% (Fig. 2, *A* and *B*). Differently, the Bin1-PL OE reduced Rab5-positive endosome size only by 10%, and the Bin1-KR OE did not alter endosome size (Fig. 2, *A* and *B*). Additionally, we analyzed endogenous EEA1, another marker of early endosomes (Fig. S1). Similarly to Rab5, we found a shrinkage of EEA1-positive endosomes upon Bin1-WT OE (18%). The PL and KR mutants induced smaller reductions in EEA1-positive endosome size, by 13% and 4%, respectively, although only the KR mutant was significantly different from Bin1-WT (Fig. S1, *A* and *B*). Of note, Bin1-WT OE led to an increase in the number of Rab5-and EEA1-positive endosomes by 22% and 24%, respectively (Fig. S1, *C* and *D*). The Bin1 mutants failed to increase the number of EEA1-positive endosomes but not Rab5-positive endosomes (Fig. S1, *C* and *D*), suggesting that the Rab5 OE compensates for the Bin1 mutants' effect on endosomes.

To remove the confounding role of endogenous Bin1, we performed a rescue experiment in which we expressed Bin1-WT and mutants upon Bin1 KD with siRNA. As reported, we found Rab5-positive endosomes 16% larger upon Bin1 KD (15, 50). Furthermore, Bin1-WT re-expression rescued Rab5-positive endosomes size, whereas Bin1-PL rescued partially, and Bin1-KR did not rescue (Fig. 2, *C* and *D*). Additionally, a heatmap of cumulative distribution (%) of endosome size is shown (Fig. 2*F*). The deepening of greater size blocks for siBin1 indicates the higher percentage of larger endosomes, similar after Bin1-KR re-expression but different from Bin1-WT and Bin1-PL re-expression.

These results suggest that the KR mutation is more pathogenic than the PL mutation, inducing a complete Bin1 loss of function in the control of early endosomes size.

Bin1 mutations reduce interaction with BACE1 and its endocytic recycling

Previously, we linked the increase in endosome size to the decreased recycling of BACE1 when Bin1 was KD (15). In addition, Miyagawa *et al*. (49) showed that Bin1 interacts with BACE1 in HeLa cells. Here, we demonstrate that Bin1 coimmunoprecipitated BACE1 from wild-type mouse brain lysates (Fig. 3*A*), supporting that Bin1 interacts with BACE1 in the brain. Moreover, we show the reverse that BACE1-GFP coimmunoprecipitated Bin1-WT from N2a cells coexpressing BACE1-GFP and Bin1-WT (Fig. 3*B*). We assessed if the LOAD mutations interfere with the Bin1 interaction with BACE1. Importantly, BACE1-GFP coimmunoprecipitated less Bin1-PL and Bin1-KR (Fig. 3*B*). Quantification showed that the BACE1-GFP tended to interact less with Bin1-PL while the interaction with Bin1-KR was significantly reduced (65%) (Fig. 3*C*), which indicates that although both mutations may interfere with Bin1 interaction with BACE1, the KR mutation has a more disruptive effect.

BACE1 trafficking could be affected by the loss of its interaction with Bin1 mutants. To confirm this hypothesis, we investigated if the LOAD mutations alter Bin1 control of BACE1 endocytic recycling. To analyze BACE1 trafficking, we performed pulse/chase assays using an antibody against FLAG (M1) in N2a cells transiently expressing BACE1 cDNA with an N-terminal FLAG-tag and a C-terminal GFP (FLAG-BACE1-GFP), as previously (15).

To measure BACE1 recycling to the plasma membrane, we pulsed N2a cells with M1 for 10 min, then we acid-stripped non-endocytosed BACE1-bound M1 and further chased endocytosed BACE1-bound M1 for 20 min (15, 58).

Firstly, we measured BACE1 endocytosis (10 min pulse) since Bin1-WT OE decreases transferrin endocytosis (59), which we confirmed (Fig. 4). Endocytosed BACE1 was delivered to EEA1-positive early endosomes (Fig. S4*A*). We found that Bin1-WT OE reduced BACE1 endocytosis by 15% (Fig. 3, *D* and *E*). The mutations in Bin1 did not alter the BACE1 endocytosis decrease induced by Bin1-WT OE (10% Bin1-PL and 15% Bin1-KR; Fig. 3, *D* and *E*). Bin1-WT likely alters endocytosis when overexpressed by sequestering necessary endocytic components since Bin1 is not required for BACE1 endocytosis (15). The LOAD mutations do not change this overexpression phenotype.

Secondly, we measured non-recycled BACE1 (Fig. 3, *F* and *G*). We found that nonrecycled BACE1 was significantly increased in cells overexpressing Bin1-PL (43%) and Bin1-KR (70%) while Bin1-WT overexpression did not alter non-recycled BACE1 as compared with control (Fig. 3*F*).
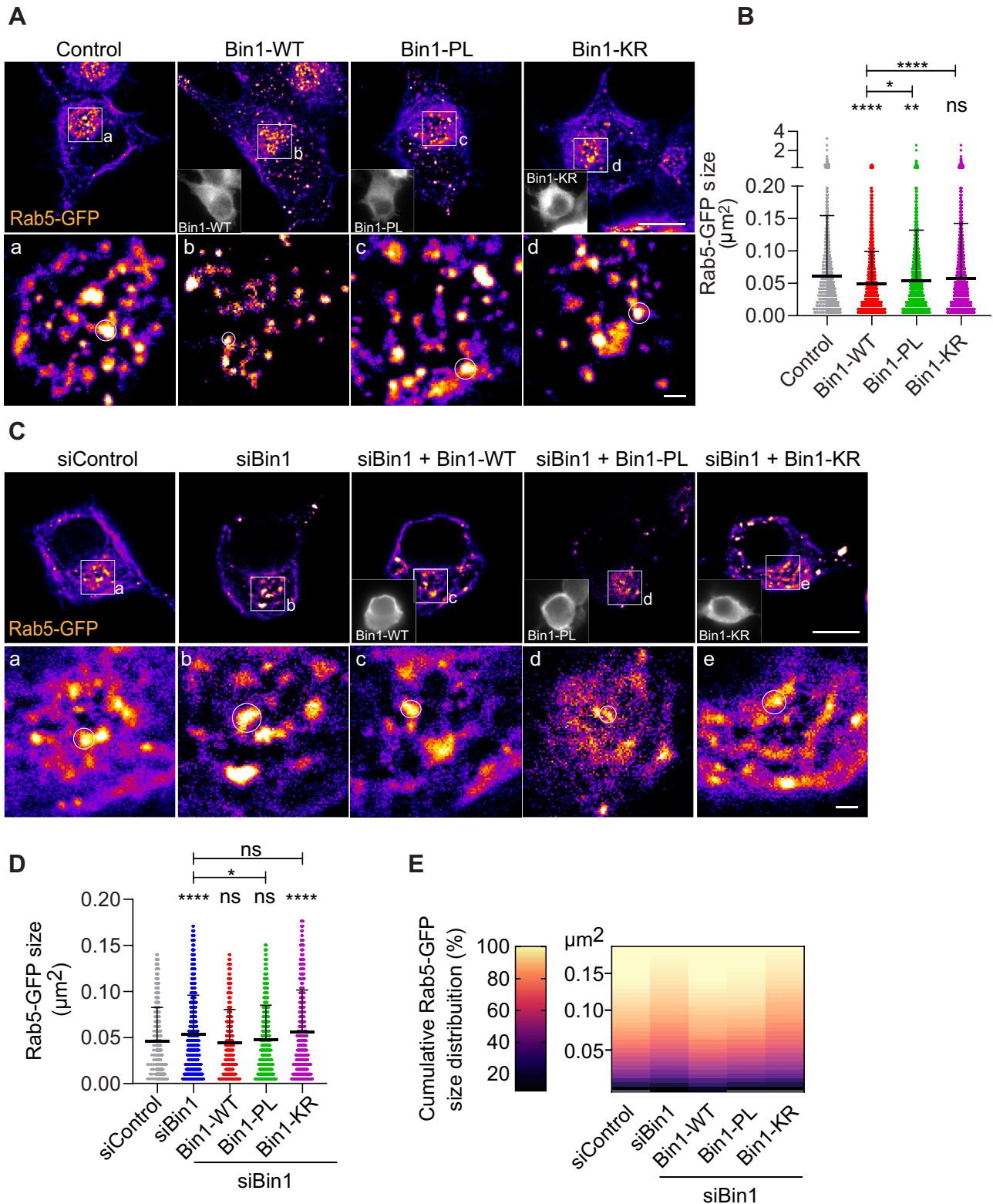
Figure 2. Bin1 mutants lose control of early endosomes size. *A,* Bin1 mutants' overexpression impact early endosomes. Rab5-GFP positive early endosomes (fire LUT) detected in N2a cells transiently expressing Rab5-GFP (control) and Bin1-WT or Bin1-PL and -KR tagged with MYC (*insets*), analyzed by epifluorescence microscopy. Images are displayed after background subtraction with Fiji. Scale bar, 10 μm. The *white squares* indicate the perinuclear region magnified in (*a–d*), where the *white circles* highlight Rab5-positive early endosomes mean size. Scale bar, 1 μm. *B,* quantification of Rab5-positive early endosomes size (μm²). (n = 3, $N_{control}$ = 96 cells, $N_{Bin1-WT}$ = 45 cells, $N_{Bin1-PL}$ = 51 cells, $N_{Bin1-KR}$ = 54 cells; ^{ns}P = 0.1409 Bin1-KR *versus* control, *p = 0.0300 Bin1-WT *versus* Bin1-PL, **p = 0.0027 Bin1-PL *versus* Control, ****p < 0.0001 Bin1-WT *versus* control, Bin1 WT *versus* Bin1 KR, one way-ANOVA with Tukey's multiple comparisons test, mean ± SD). *C,* Bin1 mutants rescue of early endosomes enlargement induced by Bin1 KD. Rab5-positive early endosomes (fire LUT) were detected in siControl- and siBin1-treated N2a cells alone or upon transient transfection with Bin1-WT, -PL and -KR tagged with MYC (*insets*), analyzed by epifluorescence microscopy. Images are displayed after background subtraction with Fiji. Scale bar, 10 μm. The *white squares* indicate the perinuclear region magnified in (*a–d*), where the white circles highlight Rab5-positive early endosomes' mean size. Scale bar, 1 μm. *D,* quantification of

The nonrecycled BACE1 is the net balance between endocytosis and recycling. Since BACE1 endocytosis decreased upon the Bin1 mutant's overexpression, the increase in nonrecycled BACE1 is likely due to the reduction in BACE1 recycling.

We showed that Bin1 KD decreases BACE1 recycling resulting in BACE1 accumulation in early endosomes (15), and Miyagawa *et al.* showed BACE1 accumulation in late endosomes/lysosomes (49). Thus, we investigated the localization of nonrecycled BACE1 upon Bin1 mutants' overexpression. Overall nonrecycled BACE1 colocalized more with EEA1-positive endosomes (40–50%) than with LAMP1-positive endosomes (10–15%). Notably, Bin1-PL and Bin1-KR overexpression increased nonrecycled BACE1 colocalization with EEA1 by 12% (Fig. 3, *H* and *I*). None of the Bin1 mutants increased colocalization with LAMP1 (Fig. 3, *J* and *K*). Bin1-WT overexpression did not affect nonrecycled BACE1 colocalization with EEA1 but increased colocalization with LAMP1 by 5% (Fig. 3, *H–K*).

Together, our results indicate that Bin1-WT OE may not alter Aβ42 accumulation because it reduces BACE1 endocytosis required for APP cleavage by BACE1 or because it increases traffic to late endosomes. In turn, both Bin1 mutants' impact on BACE1 recycling was more prominent than on its endocytosis. Consequently, the decrease of BACE1 recycling to the plasma membrane leads to BACE1 accumulation in early endosomes, where likely increases APP processing. The mechanism may be due to the reduced interaction of Bin1 with BACE1 due to LOAD mutations.

Bin1 mutants impair the canonical transferrin endocytic recycling

Since transferrin is the canonical cargo of endocytic recycling and Bin1 overexpression impairs transferrin endocytosis in nonneuronal cells (37), we next checked whether overexpression of Bin1-WT and mutants alter transferrin endocytosis and recycling, similarly to BACE1 (Fig. 3).

To follow transferrin endocytosis, we pulsed N2a cells with fluorophore-conjugated transferrin for 2 min, upon Bin1-WT, Bin1-PL, and Bin1-KR OE. We found that Bin1-WT OE reduced transferrin internalization by 25% and that when cells overexpressed Bin1-PL and Bin1-KR, there was a similar reduction in transferrin endocytosis (20%) (Fig. 4, *A* and *B*). These results indicate that Bin1-WT overexpression impairs transferrin endocytosis, which is not altered by the mutations.

To follow transferrin recycling, we chased endocytosed transferrin for 20 min after a 10 min pulse and quantified the intensity remaining intracellularly (Fig. 4, *C* and *D*). Like BACE1, Bin1-WT OE did not significantly change while the Bin1-PL OE increased substantially by 50% nonrecycled

transferrin. Unexpectedly, the Bin1-KR OE did not alter the nonrecycled transferrin.

These data indicate that transferrin recycling is reduced by Bin1-PL mutant but not by Bin1-WT or Bin1-KR. The KR mutation may affect BACE1 endocytic recycling more specifically, while the PL mutation may have a more broad effect on endocytic recycling.

Discussion

BIN1 variants were associated with LOAD, but their translation into a disease mechanism is missing. Previously, we showed that Bin1 loss of function induced by Bin1 knockdown (KD) increased Aβ42 production due to the accumulation of BACE1 at enlarged early endosomes. Mechanistically, we found that Bin1 KD reduced BACE1 recycling to the plasma membrane. Here we investigated the impact of two LOAD coding variants in BIN1 function in controlling Aβ42 production and early endosome size. We introduced the two mutations, PL and KR, in wild-type neuronal BIN1 cDNA and determined the impact of their overexpression or re-expression in neuronal cells. Bin1 mutants increased Aβ42 intracellular accumulation, failed to control early endosome size, decreased BACE1 recycling, and reduced interaction with BACE1, indicating that the two LOAD mutations are pathogenic (Fig. 5).

Intracellular Aβ

The overexpression of Bin1 mutants increased intracellular Aβ42 while, in contrast, Bin1 wild-type did not. The Bin1 mutants' phenotype was similar to that of Bin1 KD, although the mutants' effect was more modest, increasing Aβ42 by 30%, while knocking down Bin1 increased Aβ42 by 65%. The loss of Bin1 function due to the LOAD mutations was confirmed when both mutants' re-expression failed to rescue the Bin1 KD-dependent rise in Aβ42 compared with Bin1 wild-type. The impact of these two coding variants could be different from the regulatory variant (rs59335482) previously shown to increase BIN1 expression (41) since wild-type neuronal Bin1 overexpression did not impact intracellular Aβ42 accumulation. Since the increased expression of BIN1 also leads to increase levels of the ubiquitous Bin1 isoform, it remains undetermined if ubiquitous Bin1 overexpression affects intracellular Aβ42.

Interestingly, we also observed that the Bin1 mutants did not increase iAβ40, not recapitulating our previous observations that Bin1 KD increased iAβ40 although to a lesser extent than iAβ42 (15). Our results suggest an increase in the ratio Aβ42/40 in the presence of LOAD Bin1 mutations. The increase in the ratio Aβ42/40 in AD was established due to familial AD mutations in presenilins, the catalytic component of γ-secretase (60). More recent work indicates that presenilins' activity depends on the trafficking of γ-secretase to endosomes

Rab5-positive early endosomes size (μm^2) (n = 3, $N_{siControl}$ = 48 cells, N_{siBin1} = 51 cells, $N_{siBin1+Bin1-WT}$ = 31 cells, $N_{siBin1+Bin1-PL}$ = 39 cells, $N_{siBin1+Bin1-KR}$ = 36 cells; ^{ns}P > 0.9999 siBin1+Bin1-WT *versus* siControl, siBin1+Bin1-PL *versus* siControl, siBin1 vs siBin1+Bin1 KR, *p = 0.0243 siBin1 *versus* siBin1+Bin1-PL, ****p < 0.0001 siBin1 *versus* siControl, siBin1+Bin1-KR *versus* siControl, Kruskal-Wallis test, mean ± SD). *E*, cumulative Rab5-positive endosomes size (μm^2) frequency distribution. Colormap magma: 0% (*black*) to 100% (*yellow*) (n = 3; $N_{siControl}$ = 48 cells, N_{siBin1} = 51 cells, $N_{siBin1+Bin1-WT}$ = 31 cells, $N_{siBin1+Bin1-PL}$ = 39 cells, $N_{siBin1+Bin1-KR}$ = 36 cells).
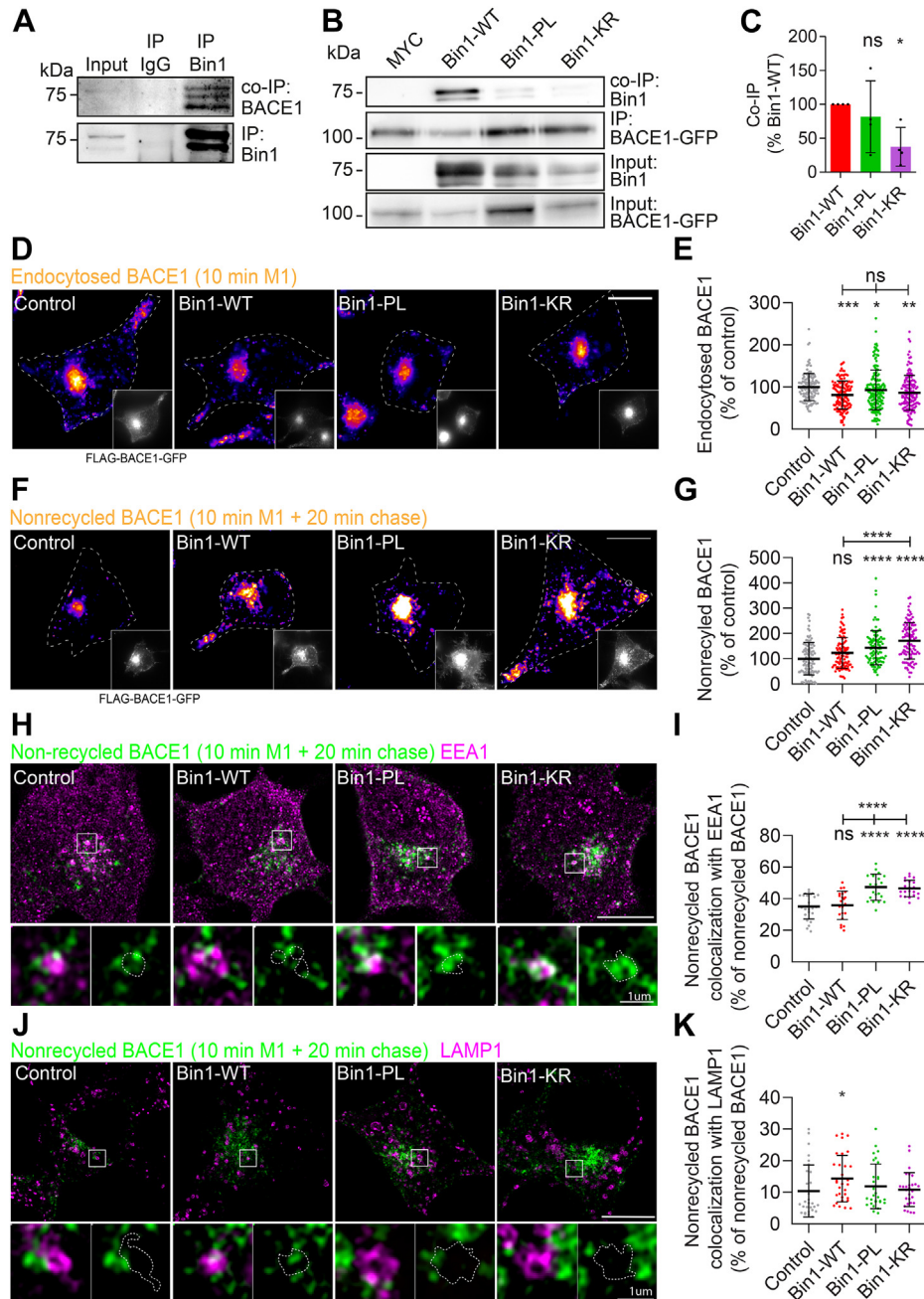
Figure 3. Bin1 mutants' impact BACE1 endocytic trafficking. *A*, BACE1 co-immunoprecipitation with Bin1 from wild-type mouse brain homogenates (input) using anti-Bin1 (IP Bin1), or normal IgG (IP IgG) detected with anti-BACE1 or anti-Bin1 antibodies (n = 3). *B*, Bin1-WT or mutants coimmunoprecipitation with BACE1-GFP from cells coexpressing BACE1-GFP and Bin1-WT, Bin1-PL or Bin1-KR (input), using GFP-traps, detected with anti-BACE1 (IP) or anti-Bin1 (Co-IP) antibodies. *C*, quantification of coimmunoprecipitated Bin1-WT or mutants normalized by immunoprecipitated BACE1 and respective inputs (n = 4, ^{ns}P = 0.3143 Bin1-PL *versus* Bin1-WT, ^{ns}P = 0.3429 Bin1-PL *versus* Bin1-KR, $*p$ = 0.0286 Bin1-WT *versus* Bin1-KR, Mann–Whitney test, mean ± SD). *D–K*, BACE1 endocytic trafficking followed in N2a cells transiently expressing BACE-GFP N-terminally tagged with FLAG (control) and Bin1-WT or Bin1-PL and -KR, using a pulse-chase assay with M1, an anti-FLAG antibody, analyzed by epifluorescence microscopy. *D*, endocytosed BACE1 (10 min M1, fire LUT) assessed by immunofluorescence in N2a cells with a secondary antibody against the endocytosed anti-FLAG (M1). *Insets* show GFP signal corresponding to FLAG-BACE1-GFP. Scale bar, 10 μm. *E*, quantification of endocytosed BACE1 (10 min M1) fluorescence normalized to FLAG-BACE1-GFP fluorescence and in the percentage of the control (n = 4, $N_{control}$ = 134 cells, $N_{Bin1-WT}$ = 137 cells, $N_{Bin1-PL}$ = 171 cells, $N_{Bin1-KR}$ = 142 cells, ^{ns}P = 0.5282 Bin1-WT *versus* Bin1-PL, $^{ns}P >$ 0.9999 Bin1-WT *versus* Bin1-KR, Bin1-PL *versus* Bin1-KR, $*p$ = 0.0404 Bin1-PL *versus* control, $**p$ = 0.0017 Bin1-KR *versus* control, $***p$ = 0.0002 Bin1-WT *versus* control, Kruskal-Wallis test, mean ± SD). *F*, nonrecycled BACE1 (fire LUT) detected upon 10 min pulse with M1 and 20 min chase, assessed by immunofluorescence in N2a cells with a secondary antibody against the endocytosed anti-FLAG (M1). *Insets* show GFP signal corresponding to FLAG-BACE1-GFP. Scale bar, 10 μm. *G*, quantification of nonrecycled BACE1 fluorescence normalized to FLAG-BACE1-GFP fluorescence and in the percentage of the control (n = 3, $N_{control}$ = 105 cells, $N_{Bin1-WT}$ = 101, $N_{Bin1-PL}$ = 104 cells, $N_{Bin1-KR}$ = 104 cells; ^{ns}P = 0.0934 Bin1-WT *versus* Control, $****p < 0.0001$ Bin1-PL *versus* control, Bin1-KR *versus* control, Bin1-WT *versus* Bin1-KR, Kruskal-Wallis test, mean ± SD). *H*, nonrecycled BACE1 (*green*, detected upon 10 min pulse with M1 and 20 min chase) localization in EEA1-positive endosomes (*magenta*), assessed by immunofluorescence in N2a cells with an antibody against endogenous EEA1. Images are displayed merged after background subtraction with Fiji. Scale bar, 10 μm. The white squares indicate magnified endosomes. Nonrecycled BACE1 is shown individually and merged with EEA1. Scale bar, 1 μm. *I*, quantification of nonrecycled BACE1 colocalization with EEA1 (n = 3, $N_{control}$ = 24 cells, $N_{Bin1-WT}$ = 22 cells, $N_{Bin1-PL}$ = 21 cells, $N_{Bin1-KR}$ = 21 cells; ^{ns}P = 0.9305 Bin1-WT *versus* control, $****p < 0.0001$ Bin1-PL *versus* control, Bin1-KR *versus* control, Bin1-WT *versus* Bin1-PL, Bin1-WT *versus* Bin1-KR, one-way ANOVA, mean ± SD). *J*, non-recycled BACE1 (*green*, detected upon 10 min pulse with M1
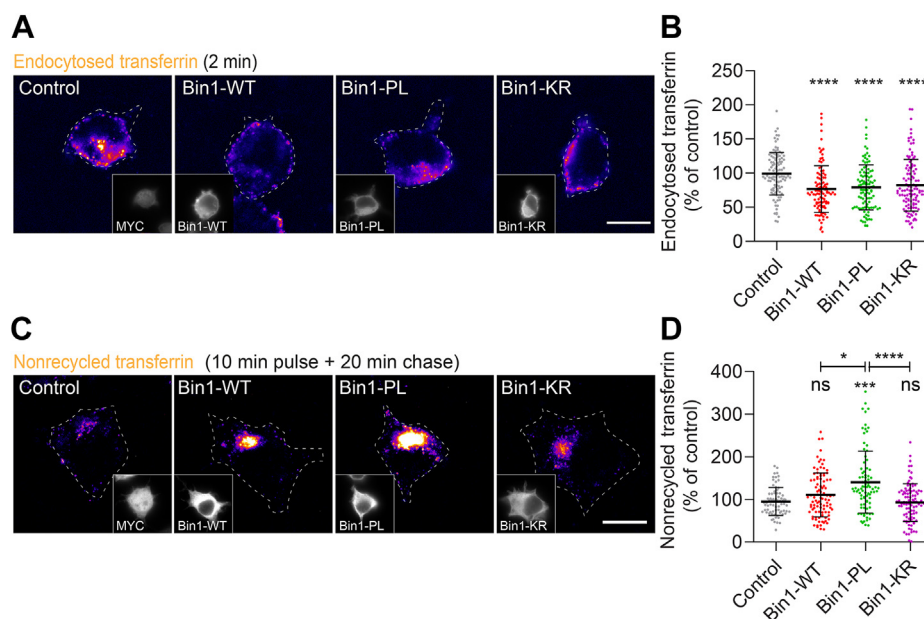
Figure 4. Bin1 mutants impair the canonical transferrin endocytic recycling. Transferrin endocytic trafficking followed in N2a cells transiently expressing MYC (control), Bin1-WT, Bin1-PL, and -KR, using a pulse-chase assay with fluorescently labeled transferrin (Alexa647-transferrin), analyzed by epifluorescence microscopy. *A*, endocytosed transferrin (2 min Alexa647-transferrin, fire LUT) detected in N2a cells. Insets show MYC signal corresponding to MYC (control), Bin1-WT, Bin1-PL, and -KR. Scale bar, 10 μm. *B*, quantification of endocytosed transferrin mean fluorescence in the percentage of control (n = 3, $N_{control}$ = 109 cells, $N_{Bin1-WT}$ = 105 cells, $N_{Bin1-PL}$ = 101 cells, $N_{Bin1-KR}$ = 111 cells; ****$p < 0.0001$ Bin1-WT *versus* control, Bin1-PL *versus* control, Bin1-KR *versus* control, Kruskal–Wallis test, mean ± SD). *C*, nonrecycled transferrin (fire) detected upon 10 min pulse with Alexa647-transferrin and 20 min chase in N2a cells. Insets show MYC signal corresponding to control, Bin1-WT, Bin1-PL, and -KR. Scale bar, 10 μm. *D*, quantification of non-recycled transferrin mean fluorescence in percentage of control (n = 3, $N_{control}$ = 76, $N_{Bin1-WT}$ = 97, $N_{Bin1-PL}$ = 88, $N_{Bin1-KR}$ = 97; $^{ns}P = 0.8713$ Bin1-WT *versus* control, $^{ns}P > 0.9999$ Bin1-KR *versus* control, *$p = 0.0265$ Bin1-WT *versus* Bin1-PL, ***$p = 0.0002$ Bin1-PL *versus* control, ****$p < 0.0001$ Bin1-PL *versus* Bin1-KR, Kruskal–Wallis test, mean ± SD).

and endosomal luminal pH ([18], [61], [62]). Thus the trafficking of γ-secretase may also be susceptible to the interference of LOAD mutations in the Bin1 control of endocytic recycling.

Early endosome size

The Bin1 wild-type overexpression reduced Rab5 and EEA1-positive early endosome size as previously reported for Rab5-positive endosomes ([50]). The overexpression of Bin1 mutants did not recapitulate Bin1 wild-type reduction of early endosome size, suggestive of a loss of function. However, their loss of function was insufficient to induce early endosomes' enlargement as observed when Bin1 is depleted. Interestingly, the rescue experiments revealed that the KR mutation in Bin1 could be more pathogenic than the PL mutation. Since Bin1-KR re-expression could not rescue Rab5-positive endosome size in cells depleted for Bin1, while the Bin1-PL re-expression partially rescued.

BACE1 endocytic recycling

Given the previously reported impact of Bin1 overexpression in transferrin endocytosis ([37], [63]), we analyzed whether Bin1 wild-type and mutants' overexpression impact

transferrin and BACE1 endocytosis in neuronal cells. Our data confirmed that Bin1, when overexpressed, interferes with endocytosis, giving a similar inhibition for transferrin and BACE1 endocytosis. However, unexpectedly, the mutations in Bin1 did not alter the decrease in endocytosis induced by Bin1 overexpression. The mechanism of BACE1 endocytosis is somewhat controversial, with reports supporting that it is clathrin-mediated, while others indicate that it is ARF-6-dependent ([7], [8]). Our results support that BACE1 undergoes clathrin-mediated endocytosis like transferrin ([64]).

The overexpression of both Bin1 mutants reduced BACE1 recycling, recapitulating the Bin1 KD phenotype, indicating that the mutations induce the loss of function of Bin1 in the control of BACE1 recycling. Accordingly, both mutations decreased Bin1 interaction with BACE1. The decrease in recycling led to increased intracellular BACE1 in early endosomes, suggesting increased BACE1 access to APP in early endosomes, processing it more. We analyzed APP processing upon Bin1 mutants' overexpression, but we found no significant change in the overall APP C-terminal fragments. The increase in beta-CTFs production is likely below the detection limit of the technique used. Unfortunately, more sensitive methods are not available for mouse APP-CTFs.

and 20 min chase) localization in LAMP1-positive endosomes (*magenta*), assessed by immunofluorescence in N2a cells with an antibody against endogenous LAMP1. Images are displayed merged after background subtraction with Fiji. Scale bar, 10 μm. The white squares indicate magnified endosomes. Non-recycled BACE1 is shown individually and merged with LAMP1. Scale bar, 1 μm. *K*, quantification of non-recycled BACE1 colocalization with LAMP1 (n = 3, $N_{control}$ = 29 cells, $N_{Bin1-WT}$ = 32 cells, $N_{Bin1-PL}$ = 30 cells, $N_{Bin1-KR}$ = 28 cells; $^{ns}P > 0.9999$ Bin1-KR *versus* control, Bin1-WT *versus* Bin1-PL, Bin1-PL *versus* Bin1-KR, $^{ns}P = 0.8539$ Bin1-PL *versus* control, $^{ns}P = 0.6546$ Bin1-WT *versus* Bin1-KR, *$p = 0.0299$ Bin1-WT *versus* control, Kruskal–Wallis test, mean ± SD).
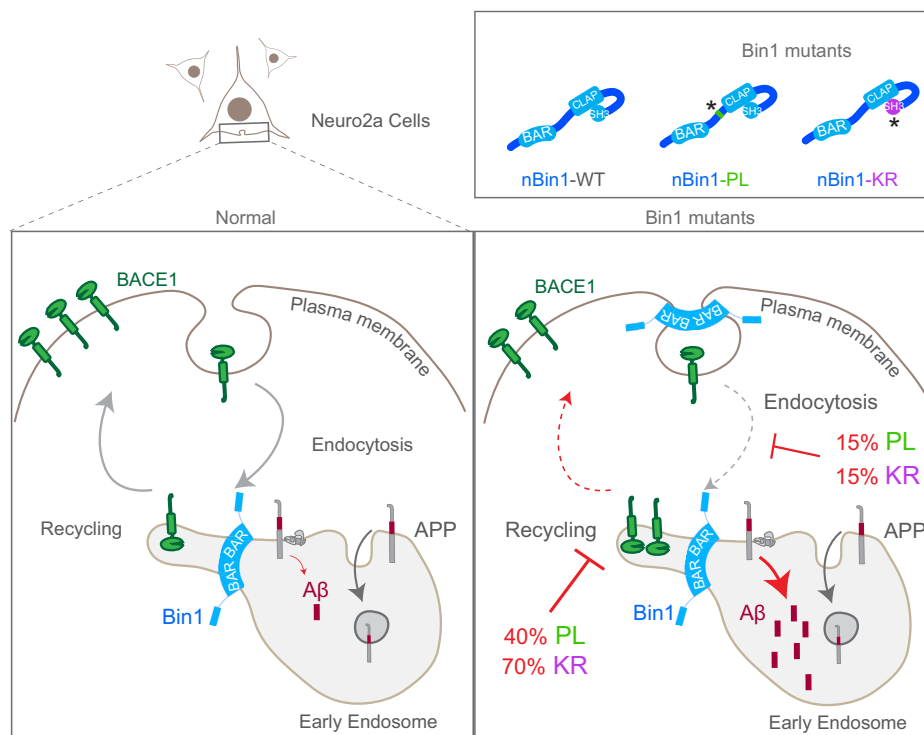
Figure 5. Schematic diagram illustrating the mechanisms used by Bin1 mutants to increase intracellular Aβ accumulation. Normally, Bin1 enables BACE1 recycling to the plasma membrane maintaining low Aβ production. The LOAD mutations PL (near CLAP domain) and KR (in the SH3 domain) in Bin1 interfere with its function in regulating BACE1 trafficking. Bin1 mutants interfere with BACE1 endocytosis but even more with its recycling—the accumulation of nonrecycled BACE1 results in more Aβ production and accumulation. KR mutation leads to a more prominent defect in BACE1 recycling than the PL mutation. Thus, their pathogenicity may impact the development of late-onset AD early mechanisms differently.

Nevertheless, we detected an increase in Aβ42 accumulation in early endosomes and late endosomes/lysosomes. Interestingly, the impact of the two mutations in Bin1 in BACE1 recycling has different magnitudes. The KR mutation has a more significant effect than the PL mutation in BACE1 recycling, which correlates with higher intracellular Aβ42.

Besides, we analyzed transferrin recycling since it decreases upon Bin1 depletion (39, 40) to determine if it was similarly affected by Bin1 mutants. Surprisingly we found that the PL mutation, but not KR, leads to decreased transferrin recycling. Thus, PL mutation likely interferes with Bin1 function in the control of endocytic recycling differently from KR mutation.

Overall, we find that the more prominent defect in BACE1 recycling plausibly overcomes the reduction in endocytosis to underlie the increase in Aβ42 production induced by mutant Bin1.

Potential mechanisms

Bin1 WT overexpression impact in reducing endocytosis

Bin1 overexpression may inhibit endocytosis by sequestering its interacting partners' clathrin, endophilin, and dynamin, indirectly compromising endocytic vesicle formation, membrane curvature, and scission, respectively (37, 63).

Bin1 mutants' impact in reducing endocytic recycling

The difference in the PL and KR Bin1 mutants' impact on endocytic recycling could be related to how the two mutations alter the Bin1 protein.

The PL mutation localizes in the proline-serine rich domain, where the lost proline could lead to an altered Bin1 secondary structure or conformation (65) or the observed reduced binding to BACE1 directly or *via* interactors (66), such as clathrin (67), which can participate in endocytic recycling (68).

The KR mutation occurs in the SH3 domain in the RT loop, one of three loops that characterize the structure of SH3 domains, composed of a patch of aromatic residues on the domain's ligand-binding face that can modulate binding typically to proline-rich domains of proteins. Indeed, Bin1 interacts through its SH3 domain with the proline-rich domain in dynamin (69, 70). Further, the replacement of arginine to lysine was observed to reduce protein-binding affinity due to conformation changes (66). Indeed, the KR mutation had a more dramatic impact in the interaction with BACE1, but the Bin1-KR interaction with dynamin, and others, may be equally reduced.

Both mutations may also interfere with neuronal Bin1 self-inhibition through the intramolecular binding between the CLAP domain and the SH3 domain (46). This intramolecular binding may function as a curvature sensor triggering Bin1 to engage with the appropriately curved membrane (71). Thus, mutations in each domain could interfere with the Bin1 localization to the tubulated recycling endosomal carriers. Alternatively, it could interfere with the binding of Bin1 directly to BACE1 or indirectly through interaction with sorting nexin 4 (SNX4) (72), which also plays a role in BACE1 (73, 74) and transferrin recycling (75, 76).

Further studies of Bin1 mutations are underway, namely identifying Bin1 mutants interactome, which should illuminate the mechanism of interfering with BACE1 recycling.

Bin1 as an AD risk factor

These results support the known function of Bin1 in BACE1 recycling at early endosomes and show how Bin1 variants associated with LOAD interfere with this function, potentiating Aβ42 production and intracellular accumulation as well as endosome enlargement. The mild loss of Bin1 PL and KR mutants' function is consistent with developing a late-onset form of AD. Future studies are underway to confirm if this intracellular accumulation of Aβ42 is sufficient to cause synaptic dysfunction, the most critical effector of AD cognitive decline.

Experimental procedures

cDNA and siRNA

We used the following DNA plasmids encoding: BACE1-GFP (15); FLAG-BACE1-GFP (15); Rab5-GFP plasmid was a gift from M. Arpin (Institut Curie); siRNA-resistant neuronal Bin1-MYC construct (brain amphiphysin II (BRAMP2); isoform 1; NP_033798.1; (15)); Bin1-PL and Bin1-KR were generated by site-directed mutagenesis (NZYtech) of siRNA-resistant neuronal Bin1-MYC (for Bin1-PL, primers 5′GAAC-CATGAGCCAGAGCTGGCCAGTGGGGCCTC′ and 5′GAGG CCCCACTGGCCAGCTCTGGCTCAT GGTTC′; for Bin1-KR primers 5′GATGAGCTGCAACTCAGAGCTGGCGATGT GGTG′ and 5′CACCACATCGCCAGCTCTGAGTTGCAG CTCATC3). All plasmids were sequenced. We used the following siRNA oligonucleotides: as siControl a nontargeting control siRNA (GeneCust) and for Bin1 knockdown, siBin1 (65,598; Thermo Fisher Scientific) (15).

Cell culture, transfections, and treatments

Neuroblastoma Neuro2a (N2a) cells (ATCCCCL-131) were a gift from Zsolt Lenkei (ESPCI-ParisTech). Cells were cultured in DMEM-GlutaMAX (Thermo Fisher Scientific) with 10% FBS (Sigma-Aldrich) at 37 °C in 5% CO_2. For cDNA expression, N2a cells were transiently transfected with 0.5 µg of cDNA with Lipofectamine 2000 (Thermo Fisher Scientific) and analyzed after 24 h. For small interfering RNA (siRNA) treatment, N2a cells were transiently transfected with 10 nM specific siRNA with Lipofectamine RNAiMax (Thermo Fisher Scientific) and analyzed after 72 h. When indicated, cDNA was transfected after 48 h of siRNA treatment, and cells were analyzed after 24 h. When indicated, BACE1 was inhibited by 9–16 h treatment with 30 µM compound IV (Calbiochem), gamma-secretase was inhibited by 9–16 h treatment with 250 nM DAPT (Calbiochem), or DMSO (solvent) was used as control. All experiments were carried out in at least three independent sets of culture, except when indicated.

Antibodies and probes

The following antibodies were used: anti-APP (Y188, Gene-Tex, cat GTX61201, 1:1000); anti-Aβ42 mAb (H31L21,

Invitrogen, cat 700254, 1:200); anti-Aβ40 pAb (Sigma, cat Ab5074P, 1:100); anti-FLAG (M1) mAb (Sigma, cat F3040, 1:100); anti-MYC pAb (1:500); anti-tubulin mAb (Tu-20, Millipore, cat MAB1637, 1:10,000); anti-EEA1 pAb (Sigma, cat E3906; 1:250); anti-EEA1 pAb (N-19, Abcam, cat sc-6415, 1:50); anti-LAMP1 mAb (BD, cat 553792, 1:200); anti-Bin1 mAb (Sigma, cat 05-449, 1:1000). The probe Alexa Fluor 647 Conjugate-transferrin (Thermo Fisher Scientific) was used in pulse-chase assays. Immunofluorescence labeling N2a cells were fixed with 4% paraformaldehyde for 10 to 15 min, permeabilized, and blocked with 0.1% saponin, 2% FBS, 1% BSA for 1 h before antibody incubation using standard procedure. For Aβ42 labeling, cells were permeabilized with 0.1% saponin for 1 h before blocking, and primary antibody incubated for 16 h. Coverslips were then mounted using Fluoromount-G (Southern Biotech).

Trafficking assays

Trafficking assays were performed as previously (15). Briefly, before endocytosis experiments, N2a cells, expressing FLAG-BACE1-GFP or not, were starved in a serum-free medium (30 min). For BACE1 endocytosis, N2a cells were incubated with anti-FLAG (M1) for 10 min. For BACE1 recycling, N2a cells pulsed with M1 were acid stripped (0.5 M NaCl, 0.2 M acetic acid; 4 s) and quickly rinsed in PBS before chasing for 20 min at 37 °C. A second acid stripping was performed before fixation, and nonrecycled proteins were immunolabeled upon permeabilization. For transferrin endocytosis, N2a cells were incubated with fluorophore-conjugated transferrin (1:100) for 2 min. For transferrin recycling, N2a cells pulsed with fluorophore-conjugated transferrin were washed in PBS (4 s) before recycling for 20 min at 37 °C. A second washing was performed before fixation.

Image acquisition

Epifluorescence microscopy was carried out on a widefield upright microscope Axio Imager.Z2 (Zeiss) equipped with a 60× NA-1.4 oil immersion objective and an AxioCam MRm CCD camera (Zeiss). Confocal microscopy was performed with LSM980 equipped with AiryScan 2.0 (Zeiss). For direct comparison, samples were imaged in parallel and using identical acquisition parameters.

Image processing and analysis

Image processing analyses were carried out using the free image analysis software: ICY (77) and FIJI (ImageJ) (78).

For the quantification of intracellular Aβ42, BACE1, and transferrin levels, regions of interest corresponding to randomly chosen single cells were outlined based on MYC labeling using the ICY "polygon type ROI (2D" tool. An ROI was also randomly chosen in an area without cells corresponding to the background. The mean fluorescence in each ROI was obtained using ICY ROI export and was presented as a percentage of the indicated control upon background fluorescence subtraction.

For the quantification of Rab5- and EEA1-positive endosomes puncta size and density per area, images were processed

using "subtract background" in FIJI. Then the endosomes were segmented using the ICY "Spot detector" plugin in each single cell ROI. The number of spots per cell ROI area was used to obtain the endosome density per area.

For the line profiles of Aβ, Bin1, and MYC, we used the "plot profile" tool in FIJI.

For the quantification of colocalizations, we used the ComDet v.0.5.5 plugin for Image J (https://github.com/ekatrukha/ComDet).

Immunoblotting

N2a cell lysates were prepared using modified RIPA buffer (50 mM Tris–HCl pH 7.4, 1% NP-40, 0.25% sodium deoxycholate, 150 mM NaCl, 1 mM EGTA, 1% SDS), with 1X PIC (Sigma-Aldrich). Sonication was performed with the settings: three cycles of 1s on and 45 ms off (pulse; total time of 30 s) at 10% amplitude. Proteins separated by 7.5, 10, or 4–12% Tris-glycine SDS–PAGE was transferred to 0.45 μm nitrocellulose membranes and processed for standard immunoblotting. HRP-conjugated secondary antibodies signal was revealed using ECL Prime kit (GE Healthcare) and captured using the ChemiDoc imager (BioRad) within the linear range and quantified by densitometry using the ImageJ software protocol (https://imagej.nih.gov/ij/docs/menus/analyze.html#gels).

Coimmunoprecipitation

Adult wild-type mice (BALB/c) cortices lysates were immunoprecipitated with anti-Bin1 or mouse IgG 16 h at 4 °C and then with 30 μl of protein G-Sepharose beads (GE Healthcare) for 3 h at 4ºC. Beads were washed 3× with lysis buffer. The sample was eluted with 2× SDS loading buffer, resolved by 7.5% Tris-Glycine SDS-PAGE, and detected by immunoblotting. Animal procedures were performed according to EU recommendations and approved by the NMS-UNL ethical committee (07/2013/CEFCM) and the national DGAV (0421/000/000/2013).

N2a cell lysates were prepared using modified RIPA buffer (50 mM Tris–HCl pH 7.4, 1% NP-40, 0.25% sodium deoxycholate, 150 mM NaCl, 1 mM EGTA, 1% SDS), with 1X PIC (Sigma-Aldrich). Lysates were immunoprecipitated with GFP-Trap Agarose beads (Chromotek) following the manufacturer protocol. Briefly, lysates were rotated with GFP-Trap Agarose beads for 1 h at 4 °C. Beads were washed three times with washing buffer (10 mM Tris-Cl pH 7.5; 100 mM NaCl; 0.5 mM EDTA; 0.05% NP-40; 1% glycerol). The IP proteins were eluted with 2× SDS loading buffer, resolved by 7.5% Tris-Glycine SDS-PAGE together with lysates (input), and detected by immunoblotting.

Statistics

GraphPad Prism 8 software was used for graph generation with mean ± SD. The sample size was determined based on pilot studies. Statistical significance for at least three independent experiments was determined on normal data (D'Agostino-Pearson omnibus normality test) by two-tailed Student's *t* test and multiple comparisons one-way ANOVA with Tukey's test using GraphPad Prism 6. Statistical significance for nonparametric data was tested by the Mann–Whitney test or, for multiple comparisons, the Kruskal–Wallis test, followed by Dunn's multiple-comparison test. Data were expressed as mean ± SD.

Data availability

Data are to be shared upon request.

knockdown; LOAD, late-onset Alzheimer's disease; N2a, Neuro2a; mAb, monoclonal antibody; OE, overexpression; pAb, polyclonal antibody; PBS, phosphate-buffered saline; PIC, protease inhibitor cocktail; RIPA, radio-immunoprecipitation assay; RVS167, reduced viability upon starvation protein 167; SDS-PAGE, sodium dodecyl sulfate–polyacrylamide gel electrophoresis; SH3, src homology 3 domain; siRNA, small interfering RNA; SNX4, sorting nexin-4.

References

1. Cataldo, A. M., Peterhoff, C. M., Troncoso, J. C., Gomez-Isla, T., Hyman, B. T., and Nixon, R. A. (2000) Endocytic pathway abnormalities precede amyloid beta deposition in sporadic Alzheimer's disease and Down syndrome: Differential effects of APOE genotype and presenilin mutations. *Am. J. Pathol.* **157**, 277–286

2. Gouras, G. K., Tsai, J., Naslund, J., Vincent, B., Edgar, M., Checler, F., Greenfield, J. P., Haroutunian, V., Buxbaum, J. D., Xu, H., Greengard, P., and Relkin, N. R. (2000) Intraneuronal Abeta42 accumulation in human brain. *Am. J. Pathol.* **156**, 15–20

3. Koo, E. H., and Squazzo, S. L. (1994) Evidence that production and release of amyloid beta-protein involves the endocytic pathway. *J. Biol. Chem.* **269**, 17386–17389

4. Vassar, R., Bennett, B. D., Babu-Khan, S., Kahn, S., Mendiaz, E. A., Denis, P., Teplow, D. B., Ross, S., Amarante, P., Loeloff, R., Luo, Y., Fisher, S., Fuller, J., Edenson, S., Lile, J., *et al.* (1999) Beta-secretase cleavage of Alzheimer's amyloid precursor protein by the transmembrane aspartic protease BACE. *Science* **286**, 735–741

5. Iizuka, T., Shoji, M., Kawarabayashi, T., Sato, M., Kobayashi, T., Tada, N., Kasai, K., Matsubara, E., Watanabe, M., Tomidokoro, Y., and Hirai, S. (1996) Intracellular generation of amyloid beta-protein from amyloid beta-protein precursor fragment by direct cleavage with beta- and gamma-secretase. *Biochem. Biophys. Res. Commun.* **218**, 238–242

6. Urmoneit, B., Reinsch, C., Turner, J., Czech, C., Beyreuther, K., and Dyrks, T. (1995) Inhibition of beta A4 production by specific modulation of beta-secretase activity. *J. Mol. Neurosci.* **6**, 23–32

7. Sannerud, R., Declerck, I., Peric, A., Raemaekers, T., Menendez, G., Zhou, L., Veerle, B., Coen, K., Munck, S., De Strooper, B., Schiavo, G., and Annaert, W. (2011) ADP ribosylation factor 6 (ARF6) controls amyloid precursor protein (APP) processing by mediating the endosomal sorting of BACE1. *Proc. Natl. Acad. Sci. U. S. A.* **108**, E559–E568

8. Chia, P. Z. C., Toh, W. H., Sharples, R., Gasnereau, I., Hill, A. F., and Gleeson, P. A. (2013) Intracellular itinerary of internalised β-secretase, BACE1, and its potential impact on β-amyloid peptide biogenesis. *Traffic* **14**, 997–1013

9. Cirrito, J. R., Kang, J.-E., Lee, J., Stewart, F. R., Verges, D. K., Silverio, L. M., Bu, G., Mennerick, S., and Holtzman, D. M. (2008) Endocytosis is required for synaptic activity-dependent release of amyloid-beta *in vivo*. *Neuron* **58**, 42–51

10. Rajendran, L., Schneider, A., Schlechtingen, G., Weidlich, S., Ries, J., Braxmeier, T., Schwille, P., Schulz, J. B., Schroeder, C., Simons, M., Jennings, G., Knölker, H.-J., and Simons, K. (2008) Efficient inhibition of the Alzheimer's disease beta-secretase by membrane targeting. *Science* **320**, 520–523

11. Zou, L., Wang, Z., Shen, L., Bao, G. B., Wang, T., Kang, J. H., and Pei, G. (2007) Receptor tyrosine kinases positively regulate BACE activity and amyloid-beta production through enhancing BACE internalization. *Cell Res.* **17**, 389–401

12. Refolo, L. M., Sambamurti, K., Efthimiopoulos, S., Pappolla, M. A., and Robakis, N. K. (1995) Evidence that secretase cleavage of cell surface Alzheimer amyloid precursor occurs after normal endocytic internalization. *J. Neurosci. Res.* **40**, 694–706

13. Edgar, J. R., Willén, K., Gouras, G. K., and Futter, C. E. (2015) ESCRTs regulate amyloid precursor protein sorting in multivesicular bodies and intracellular amyloid-β accumulation. *J. Cell Sci.* **128**, 2520–2528

14. Morel, E., Chamoun, Z., Lasiecka, Z. M., Chan, R. B., Williamson, R. L., Vetanovetz, C., Dall'Armi, C., Simoes, S., Point Du Jour, K. S., McCabe, B. D., Small, S. A., and Di Paolo, G. (2013) Phosphatidylinositol-3-phosphate regulates sorting and processing of amyloid precursor protein through the endosomal system. *Nat. Commun.* **4**, 2250

15. Ubelmann, F., Burrinha, T., Salavessa, L., Gomes, R., Ferreira, C., Moreno, N., and Guimas Almeida, C. (2017) Bin1 and CD2AP polarise the endocytic generation of beta-amyloid. *EMBO Rep.* **18**, 102–122

16. Rovelet-Lecrux, A., Hannequin, D., Raux, G., Le Meur, N., Laquerrière, A., Vital, A., Dumanchin, C., Feuillette, S., Brice, A., Vercelletto, M., Dubas, F., Frebourg, T., and Campion, D. (2006) APP locus duplication causes autosomal dominant early-onset Alzheimer disease with cerebral amyloid angiopathy. *Nat. Genet.* **38**, 24–26

17. Citron, M., Oltersdorf, T., Haass, C., McConlogue, L., Hung, A. Y., Seubert, P., Vigo-Pelfrey, C., Lieberburg, I., and Selkoe, D. J. (1992) Mutation of the beta-amyloid precursor protein in familial Alzheimer's disease increases beta-protein production. *Nature* **360**, 672–674

18. Sannerud, R., Esselens, C., Ejsmont, P., Mattera, R., Rochin, L., Tharkeshwar, A. K., De Baets, G., De Wever, V., Habets, R., Baert, V., Vermeire, W., Michiels, C., Groot, A. J., Wouters, R., Dillen, K., *et al.* (2016) Restricted location of PSEN2/γ-secretase determines substrate specificity and generates an intracellular Aβ pool. *Cell* **166**, 193–208

19. Knobloch, M., Konietzko, U., Krebs, D. C., and Nitsch, R. M. (2007) Intracellular Abeta and cognitive deficits precede beta-amyloid deposition in transgenic arcAbeta mice. *Neurobiol. Aging* **28**, 1297–1306

20. Takahashi, R. H., Almeida, C. G., Kearney, P. F., Yu, F., Lin, M. T., Milner, T. A., and Gouras, G. K. (2004) Oligomerization of Alzheimer's beta-amyloid within processes and synapses of cultured neurons and brain. *J. Neurosci.* **24**, 3592–3599

21. Almeida, C. G., Takahashi, R. H., and Gouras, G. K. (2006) Beta-amyloid accumulation impairs multivesicular body sorting by inhibiting the ubiquitin-proteasome system. *J. Neurosci.* **26**, 4277–4288

22. Jin, L.-W., Shie, F.-S., Maezawa, I., Vincent, I., and Bird, T. (2004) Intracellular accumulation of amyloidogenic fragments of amyloid-beta precursor protein in neurons with Niemann-Pick type C defects is associated with endosomal abnormalities. *Am. J. Pathol.* **164**, 975–985

23. Yang, A. J., Chandswangbhuvana, D., Margol, L., and Glabe, C. G. (1998) Loss of endosomal/lysosomal membrane impermeability is an early event in amyloid Abeta1-42 pathogenesis. *J. Neurosci. Res.* **52**, 691–698

24. Seshadri, S., Fitzpatrick, A. L., Ikram, M. A., DeStefano, A. L., Gudnason, V., Boada, M., Bis, J. C., Smith, A. V., Carassquillo, M. M., Lambert, J. C., Harold, D., Schrijvers, E. M. C., Ramirez-Lorca, R., Debette, S., Longstreth, W. T., *et al.* (2010) Genome-wide analysis of genetic loci associated with Alzheimer disease. *JAMA* **303**, 1832–1840

25. Wijsman, E. M., Pankratz, N. D., Choi, Y., Rothstein, J. H., Faber, K. M., Cheng, R., Lee, J. H., Bird, T. D., Bennett, D. A., Diaz-Arrastia, R., Goate, A. M., Farlow, M., Ghetti, B., Sweet, R. A., Foroud, T. M., *et al.* (2011) Genome-wide association of familial late-onset Alzheimer's disease replicates BIN1 and CLU and nominates CUGBP2 in interaction with APOE. *PLoS Genet.* **7**, e1001308

26. Hu, X., Pickering, E., Liu, Y. C., Hall, S., Fournier, H., Katz, E., Dechairo, B., John, S., Van Eerdewegh, P., Soares, H., and Alzheimer's Disease Neuroimaging Initiative (2011) Meta-analysis for genome-wide association study identifies multiple variants at the BIN1 locus associated with late-onset Alzheimer's disease. *PLoS One* **6**, e16616

27. Lee, J. H., Cheng, R., Barral, S., Reitz, C., Medrano, M., Lantigua, R., Jiménez-Velazquez, I. Z., Rogaeva, E., St George-Hyslop, P. H., and Mayeux, R. (2011) Identification of novel loci for Alzheimer disease and replication of CLU, PICALM, and BIN1 in Caribbean Hispanic individuals. *Arch. Neurol.* **68**, 320–328

28. Kamboh, M. I., Demirci, F. Y., Wang, X., Minster, R. L., Carrasquillo, M. M., Pankratz, V. S., Younkin, S. G., Saykin, A. J., Alzheimer's Disease Neuroimaging Initiative, Jun, G., Baldwin, C., Logue, M. W., Buros, J., Farrer, L., Pericak-Vance, M. A., *et al.* (2012) Genome-wide association study of Alzheimer's disease. *Transl. Psychiatry* **2**, e117

29. Lambert, J. C., Ibrahim-Verbaas, C. A., Harold, D., Naj, A. C., Sims, R., Bellenguez, C., DeStafano, A. L., Bis, J. C., Beecham, G. W., Grenier-Boley, B., Russo, G., Thorton-Wells, T. A., Jones, N., Smith, A. V., Chouraki, V., *et al.* (2013) Meta-analysis of 74,046 individuals identifies 11 new susceptibility loci for Alzheimer's disease. *Nat. Genet.* **45**, 1452–1458

30. Almeida, J. F. F., Dos Santos, L. R., Trancozo, M., and de Paula, F. (2018) Updated meta-analysis of BIN1, CR1, MS4A6A, CLU, and ABCA7 variants in Alzheimer's disease. *J. Mol. Neurosci.* **64**, 471–477

31. Tan, M.-S., Yu, J.-T., and Tan, L. (2013) Bridging integrator 1 (BIN1): Form, function, and Alzheimer's disease. *Trends Mol. Med.* **19**, 594–603

32. Peter, B. J., Kent, H. M., Mills, I. G., Vallis, Y., Butler, P. J. G., Evans, P. R., and McMahon, H. T. (2004) BAR domains as sensors of membrane curvature: The amphiphysin BAR structure. *Science* **303**, 495–499

33. Casal, E., Federici, L., Zhang, W., Fernandez-Recio, J., Priego, E.-M., Miguel, R. N., DuHadaway, J. B., Prendergast, G. C., Luisi, B. F., and Laue, E. D. (2006) The crystal structure of the BAR domain from human Bin1/ amphiphysin II and its implications for molecular recognition. *Biochemistry* **45**, 12917–12928

34. Butler, M. H., David, C., Ochoa, G. C., Freyberg, Z., Daniell, L., Grabs, D., Cremona, O., and De Camilli, P. (1997) Amphiphysin II (SH3P9; BIN1), a member of the amphiphysin/Rvs family, is concentrated in the cortical cytomatrix of axon initial segments and nodes of ranvier in brain and around T tubules in skeletal muscle. *J. Cell Biol.* **137**, 1355–1367

35. Leprince, C., Romero, F., Cussac, D., Vayssiere, B., Berger, R., Tavitian, A., and Camonis, J. H. (1997) A new member of the amphiphysin family connecting endocytosis and signal transduction pathways. *J. Biol. Chem.* **272**, 15101–15105

36. Ramjaun, A. R., Micheva, K. D., Bouchelet, I., and McPherson, P. S. (1997) Identification and characterization of a nerve terminal-enriched amphiphysin isoform. *J. Biol. Chem.* **272**, 16700–16706

37. Wigge, P., Köhler, K., Vallis, Y., Doyle, C. A., Owen, D., Hunt, S. P., and McMahon, H. T. (1997) Amphiphysin heterodimers: Potential role in clathrin-mediated endocytosis. *Mol. Biol. Cell* **8**, 2003–2015

38. Ramjaun, A. R., and McPherson, P. S. (1998) Multiple amphiphysin II splice variants display differential clathrin binding: Identification of two distinct clathrin-binding sites. *J. Neurochem.* **70**, 2369–2376

39. Muller, A. J., Baker, J. F., DuHadaway, J. B., Ge, K., Farmer, G., Donover, P. S., Meade, R., Reid, C., Grzanna, R., Roach, A. H., Shah, N., Soler, A. P., and Prendergast, G. C. (2003) Targeted disruption of the murine Bin1/ Amphiphysin II gene does not disable endocytosis but results in embryonic cardiomyopathy with aberrant myofibril formation. *Mol. Cell. Biol.* **23**, 4295–4306

40. Pant, S., Sharma, M., Patel, K., Caplan, S., Carr, C. M., and Grant, B. D. (2009) AMPH-1/Amphiphysin/Bin1 functions with RME-1/Ehd1 in endocytic recycling. *Nat. Cell Biol.* **11**, 1399–1410

41. Chapuis, J., Hansmannel, F., Gistelinck, M., Mounier, A., Van Cauwenberghe, C., Kolen, K. V., Geller, F., Sottejeau, Y., Harold, D., Dourlen, P., Grenier-Boley, B., Kamatani, Y., Delepine, B., Demiautte, F., Zelenika, D., *et al.* (2013) Increased expression of BIN1 mediates Alzheimer genetic risk by modulating tau pathology. *Mol. Psychiatry* **18**, 1225–1234

42. Karch, C. M., Jeng, A. T., Nowotny, P., Cady, J., Cruchaga, C., and Goate, A. M. (2012) Expression of novel Alzheimer's disease risk genes in control and Alzheimer's disease brains. *PLoS One* **7**, e50976

43. De Rossi, P., Andrew, R. J., Musial, T. F., Buggia-Prevot, V., Xu, G., Ponnusamy, M., Ly, H., Krause, S. V., Rice, R. C., de l'Estoile, V., Valin, T., Salem, S., Despa, F., Borchelt, D. R., Bindokas, V. P., *et al.* (2019) Aberrant accrual of BIN1 near Alzheimer's disease amyloid deposits in transgenic models. *Brain Pathol.* **29**, 485–501

44. Glennon, E. B. C., Whitehouse, I. J., Miners, J. S., Kehoe, P. G., Love, S., Kellett, K. A. B., and Hooper, N. M. (2013) BIN1 is decreased in sporadic but not familial Alzheimer's disease or in aging. *PLoS One* **8**, e78806

45. Glennon, E. B., Lau, D. H.-W., Gabriele, R. M. C., Taylor, M. F., Troakes, C., Opie-Martin, S., Elliott, C., Killick, R., Hanger, D. P., Perez-Nievas, B. G., and Noble, W. (2020) Bridging integrator-1 protein loss in Alzheimer's disease promotes synaptic tau accumulation and disrupts tau release. *Brain Commun.* **2**, fcaa011

46. Sartori, M., Mendes, T., Desai, S., Lasorsa, A., Herledan, A., Malmanche, N., Mäkinen, P., Marttinen, M., Malki, I., Chapuis, J., Flaig, A., Vreulx, A.-C., Ciancia, M., Amouyel, P., Leroux, F., *et al.* (2019) BIN1 recovers tauopathy-induced long-term memory deficits in mice and interacts with Tau through Thr348 phosphorylation. *Acta Neuropathol.* **138**, 631–652

47. Holler, C. J., Davis, P. R., Beckett, T. L., Platt, T. L., Webb, R. L., Head, E., and Murphy, M. P. (2014) Bridging integrator 1 (BIN1) protein expression increases in the Alzheimer's disease brain and correlates with neurofibrillary tangle pathology. *J. Alzheimers Dis.* **42**, 1221–1227

48. De Rossi, P., Buggia-Prévot, V., Clayton, B. L. L., Vasquez, J. B., van Sanford, C., Andrew, R. J., Lesnick, R., Botté, A., Deyts, C., Salem, S., Rao, E., Rice, R. C., Parent, A., Kar, S., Popko, B., *et al.* (2016) Predominant expression of Alzheimer's disease-associated BIN1 in mature oligodendrocytes and localization to white matter tracts. *Mol. Neurodegener.* **11**, 59

49. Miyagawa, T., Ebinuma, I., Morohashi, Y., Hori, Y., Young Chang, M., Hattori, H., Maehara, T., Yokoshima, S., Fukuyama, T., Tsuji, S., Iwatsubo, T., Prendergast, G. C., and Tomita, T. (2016) BIN1 regulates BACE1 intracellular trafficking and amyloid-β production. *Hum. Mol. Genet.* **25**, 2948–2958

50. Calafate, S., Flavin, W., Verstreken, P., and Moechars, D. (2016) Loss of bin1 promotes the propagation of tau pathology. *Cell Rep.* **17**, 931–940

51. Andrew, R. J., De Rossi, P., Nguyen, P., Kowalski, H. R., Recupero, A. J., Guerbette, T., Krause, S. V., Rice, R. C., Laury-Kleintop, L., Wagner, S. L., and Thinakaran, G. (2019) Reduction of the expression of the late-onset Alzheimer's disease (AD) risk-factor BIN1 does not affect amyloid pathology in an AD mouse model. *J. Biol. Chem.* **294**, 4477–4487

52. Gouras, G. K., Willén, K., and Tampellini, D. (2012) Critical role of intraneuronal Aβ in Alzheimer's disease: Technical challenges in studying intracellular Aβ. *Life Sci.* **91**, 1153–1158

53. Vardarajan, B. N., Ghani, M., Kahn, A., Sheikh, S., Sato, C., Barral, S., Lee, J. H., Cheng, R., Reitz, C., Lantigua, R., Reyes-Dumeyer, D., Medrano, M., Jimenez-Velazquez, I. Z., Rogaeva, E., St George-Hyslop, P., *et al.* (2015) Rare coding mutations identified by sequencing of Alzheimer disease genome-wide association studies loci. *Ann. Neurol.* **78**, 487–498

54. Barral, S., Bird, T., Goate, A., Farlow, M. R., Diaz-Arrastia, R., Bennett, D. A., Graff-Radford, N., Boeve, B. F., Sweet, R. A., Stern, Y., Wilson, R. S., Foroud, T., Ott, J., Mayeux, R., and National Institute on Aging Late-Onset Alzheimer's Disease Genetics Study (2012) Genotype patterns at PICALM, CR1, BIN1, CLU, and APOE genes are associated with episodic memory. *Neurology* **78**, 1464–1471

55. Tan, M.-S., Yu, J.-T., Jiang, T., Zhu, X.-C., Guan, H.-S., and Tan, L. (2014) Genetic variation in BIN1 gene and Alzheimer's disease risk in Han Chinese individuals. *Neurobiol. Aging* **35**, 1781.e1–1781.e8

56. Burrinha, T., Martinsson, I., Gomes, R., Terrasso, A. P., Gouras, G. K., and Almeida, C. G. (2021) Upregulation of APP endocytosis by neuronal aging drives amyloid-dependent synapse loss. *J. Cell Sci.* **134**

57. Kuperstein, I., Broersen, K., Benilova, I., Rozenski, J., Jonckheere, W., Debulpaep, M., Vandersteen, A., Segers-Nolten, I., Van Der Werf, K., Subramaniam, V., Braeken, D., Callewaert, G., Bartic, C., D'Hooge, R., Martins, I. C., *et al.* (2010) Neurotoxicity of Alzheimer's disease Aβ peptides is induced by small changes in the Aβ42 to Aβ40 ratio. *EMBO J.* **29**, 3408–3420

58. Ubelmann, F., Burrinha, T., and Guimas Almeida, C. (2017) Measuring the endocytic recycling of amyloid precursor protein (APP) in neuro2a cells. *Bio Protoc.* **7**

59. Wigge, P., and McMahon, H. T. (1998) The amphiphysin family of proteins and their role in endocytosis at the synapse. *Trends Neurosci.* **21**, 339–344

60. Wolfe, M. S. (2019) Dysfunctional γ-secretase in familial Alzheimer's disease. *Neurochem. Res.* **44**, 5–11

61. Cai, T., Hatano, A., Kanatsu, K., and Tomita, T. (2020) Histidine 131 in presenilin 1 is the pH-sensitive residue that causes the increase in Aβ42 level in acidic pH. *J. Biochem.* **167**, 463–471

62. Morais, V. A., Leight, S., Pijak, D. S., Lee, V. M.-Y., and Costa, J. (2008) Cellular localization of Nicastrin affects amyloid beta species production. *FEBS Lett.* **582**, 427–433

63. Owen, D. J., Wigge, P., Vallis, Y., Moore, J. D., Evans, P. R., and McMahon, H. T. (1998) Crystal structure of the amphiphysin-2 SH3 domain and its role in the prevention of dynamin ring formation. *EMBO J.* **17**, 5273–5285

64. Maxfield, F. R., and McGraw, T. E. (2004) Endocytic recycling. *Nat. Rev. Mol. Cell Biol.* **5**, 121–132

65. Betts, M. J., and Russell, R. B. (2003). In: Barnes, M. R., Gray, I. C., eds. *Bioinformatics for Geneticists*, John Wiley & Sons, Ltd, Chichester, UK: 289–316

66. Wu, X., Knudsen, B., Feller, S. M., Zheng, J., Sali, A., Cowburn, D., Hanafusa, H., and Kuriyan, J. (1995) Structural basis for the specific interaction of lysine-containing proline-rich peptides with the N-terminal SH3 domain of c-Crk. *Structure* **3**, 215–226

67. Evergren, E., Marcucci, M., Tomilin, N., Löw, P., Slepnev, V., Andersson, F., Gad, H., Brodin, L., De Camilli, P., and Shupliakov, O. (2004) Amphiphysin is a component of clathrin coats formed during synaptic vesicle recycling at the lamprey giant synapse. *Traffic* **5**, 514–528

68. Zhao, Y., and Keen, J. H. (2008) Gyrating clathrin: Highly dynamic clathrin structures involved in rapid receptor recycling. *Traffic* **9**, 2253–2264

69. Mayer, B. J., and Eck, M. J. (1995) SH3 domains. Minding your p's and q's. *Curr. Biol.* **5**, 364–367

70. Nicot, A.-S., Toussaint, A., Tosch, V., Kretz, C., Wallgren-Pettersson, C., Iwarsson, E., Kingston, H., Garnier, J.-M., Biancalana, V., Oldfors, A., Mandel, J.-L., and Laporte, J. (2007) Mutations in amphiphysin 2 (BIN1) disrupt interaction with dynamin 2 and cause autosomal recessive centronuclear myopathy. *Nat. Genet.* **39**, 1134–1139

71. Safari, F., and Suetsugu, S. (2012) The BAR domain superfamily proteins from subcellular structures to human diseases. *Membranes (Basel)* **2**, 91–117

72. Leprince, C., Le Scolan, E., Meunier, B., Fraisier, V., Brandon, N., De Gunzburg, J., and Camonis, J. (2003) Sorting nexin 4 and amphiphysin 2, a new partnership between endocytosis and intracellular trafficking. *J. Cell Sci.* **116**, 1937–1948

73. Kim, N.-Y., Cho, M.-H., Won, S.-H., Kang, H.-J., Yoon, S.-Y., and Kim, D.-H. (2017) Sorting nexin-4 regulates β-amyloid production by modulating β-site-activating cleavage enzyme-1. *Alzheimers Res. Ther.* **9**, 4

74. Toh, W. H., Chia, P. Z. C., Hossain, M. I., and Gleeson, P. A. (2018) GGA1 regulates signal-dependent sorting of BACE1 to recycling endosomes, which moderates Aβ production. *Mol. Biol. Cell* **29**, 191–208

75. Traer, C. J., Rutherford, A. C., Palmer, K. J., Wassmer, T., Oakley, J., Attar, N., Carlton, J. G., Kremerskothen, J., Stephens, D. J., and Cullen, P. J. (2007) SNX4 coordinates endosomal sorting of TfnR with dynein-mediated transport into the endocytic recycling compartment. *Nat. Cell Biol.* **9**, 1370–1380

76. Sakane, H., Horii, Y., Nogami, S., Kawano, Y., Kaneko-Kawano, T., and Shirataki, H. (2014) α-Taxilin interacts with sorting nexin 4 and participates in the recycling pathway of transferrin receptor. *PLoS One* **9**, e93509

77. de Chaumont, F., Dallongeville, S., Chenouard, N., Hervé, N., Pop, S., Provoost, T., Meas-Yedid, V., Pankajakshan, P., Lecomte, T., Le Montagner, Y., Lagache, T., Dufour, A., and Olivo-Marin, J.-C. (2012) Icy: An open bioimage informatics platform for extended reproducible research. *Nat. Methods* **9**, 690–696

78. Schindelin, J., Arganda-Carreras, I., Frise, E., Kaynig, V., Longair, M., Pietzsch, T., Preibisch, S., Rueden, C., Saalfeld, S., Schmid, B., Tinevez, J.-Y., White, D. J., Hartenstein, V., Eliceiri, K., Tomancak, P., *et al.* (2012) Fiji: An open-source platform for biological-image analysis. *Nat. Methods* **9**, 676–682